Wearable Metasurface-Enabled Quasi-Yagi Antenna for UHF RFID Reader With End-Fire Radiation Along the Forearm

SHAHBAZ AHMED, (Student Member, IEEE), **DUC LE**, (Student Member, IEEE),
LAURI SYDÄNHEIMO, (Member, IEEE), **LEENA UKKONEN**, (Member, IEEE),
AND TONI BJÖRNINEN, (Senior Member, IEEE)

Faculty of Medicine and Health Technology, Tampere University, 33720 Tampere, Finland

Corresponding author: Shahbaz Ahmed (shahbaz.ahmed@tuni.fi)

ABSTRACT We present a quasi-Yagi antenna mounted on a periodic surface for a wearable UHF RFID reader operating in the UHF RFID frequency band centered at 915 MHz. The periodic surface was co-optimized with the antenna to enhance the launching of surface waves to enable the end-fire radiation along the forearm so that a user can identify objects by pointing her/his hand towards them. In addition to the radiation pattern modification, the ground plane of the periodic surface serves the second purpose of isolating the antenna from the human body. We optimized the antenna in a full-wave EM simulator using a simplified cylindrical model of the forearm and in the simulation, it achieved the end-fire directivity of 5.9 dBi along the forearm. In the wireless testing, the quasi-Yagi antenna provided the read range of 3.8 m for a typical UHF RFID tag having 0 dBi gain when the reader's output power was 32 dBm that corresponds with EIRP = 0.56 W and SAR = 0.191 W/kg in our simulations. Considering both, the RFID emission regulations with EIRP = 3.28 W or 4 W and the SAR limit of 1.6 W/kg averaged over 1 gram of tissue, the read range could be further enhanced for reader units with higher output power.

INDEX TERMS Wearable antenna, Yagi antenna, surface wave antenna, periodic surface, UHF RFID, wireless body-area systems.

I. INTRODUCTION

During the past two decades, the versatile passive ultra-high frequency radio-frequency identification technology (UHF RFID) has been researched and developed for numerous applications that extend beyond identification to applications such as wireless sensing [1]–[5] and RFID based real-time localization and tracking of assets [6]–[10]. Most recently, RFID technology has been found a compelling approach to wireless body area systems [11]–[15] where it can be utilized, for instance, in wireless health applications [16]–[20]. Here either the tags, readers, or both, may be integrated into clothing. In this regard, much research has been conducted for achieving efficient and seamlessly cloth-integrable antennas for UHF RFID tags [21]–[25]. However, antennas for

The associate editor coordinating the review of this manuscript and approving it for publication was Chan Hwang See.

wearable RFID readers remain relatively less studied, yet they have been gaining more attention in the recent years [26]–[29].

The fundamental challenge in optimizing wearable antennas is the mitigation of the negative impact arising from the electromagnetic (EM) interaction between the antenna and the dissipative biological tissue. In contrast to wearable passive tags, which are not active transmitters but backscatter the reader's signal, the reader antenna transmits relatively high-power levels up to 4 W EIRP depending on the governing RFID emission regulations. Thus, the EM optimization of a reader antenna must also consider the specific absorption rate (SAR) in conjunction with the regular antenna performance parameters [30].

In the previous research, wearable reader antennas attached to gloves [28], wrapped around the wrist [27] and ankle [26] have been studied. They all read the tags from a direction

TABLE 1. Dielectric properties of body tissue at 915 Mhz [34].

Tissue	σ (S/m)	ε_r
Skin	0.8555	41.587
Fat	0.050242	5.4673
Muscle	0.93146	55.114
Bone	0.13926	12.486

orthogonal to the body surface where the reader antenna is worn. However, few wearable antennas with end-fire radiation along the body surface have been reported. A wearable quasi-Yagi near-field UHF RFID reader antenna with end-fire radiation properties integrated into a smart glove is reported in [29], [31]. Through the analysis of the near electric and magnetic fields, the authors confirmed the end-fire property, and in experiments, the attainable tag read range was found to be 0.33 m.

In our earlier work [32], we developed a head-worn quasi-Yagi RFID tag, where the antenna included a periodic surface made up of a 2-by-2 grid of square loops. By applying the folding technique, we achieved the small antenna size of 0.25λ × 0.25λ at 915 MHz or 80 mm × 80 mm, which befits the human head. However, the antenna in this work was developed for RFID tags. As a specific feature and inductive loop was included in the driven element to achieve complex conjugate impedance matching between the antenna and the RFID IC. In another study [28], the authors developed a slotted patch and a split ring resonator RFID reader antenna integrated into work gloves. The antennas exhibit a broadside radiation pattern pointing in the direction approximately orthogonal to the hand's back. The ground plane in the slotted patch antenna suppressed the antenna-body coupling and thereby enabled better EM performance and the tag read range of 3 m with a transmission power of 30 dBm.

In this paper, we present a wearable quasi-Yagi reader antenna on a textile substrate conforming to the forearm. The antenna's radiation pattern is directive along the arm so that a user can identify objects by pointing her/his hand towards them. The novel feature of the end-fire radiation pattern along the body surface is achieved by inserting a periodic surface between the antenna and the arm and co-optimizing the two for a maximally directive radiation pattern. This way the end-fire directivity is enhanced by the periodic surface that supports the launching of the surface waves at the operating frequency of the antenna.

II. HUMAN BODY MODEL AND ANTENNA MODELLING

The human body comprises various biological materials exhibiting electrical conductivity and relative permittivity tens of times higher than most conventional electronics materials [34]. The human forearm includes multiple tissue types, such as skin, fat, muscle, and bone. Although the associated dielectric properties are available in the literature (see Table 1), in practice, the thicknesses of these layers are difficult to measure and are subjective to the human anatomy.
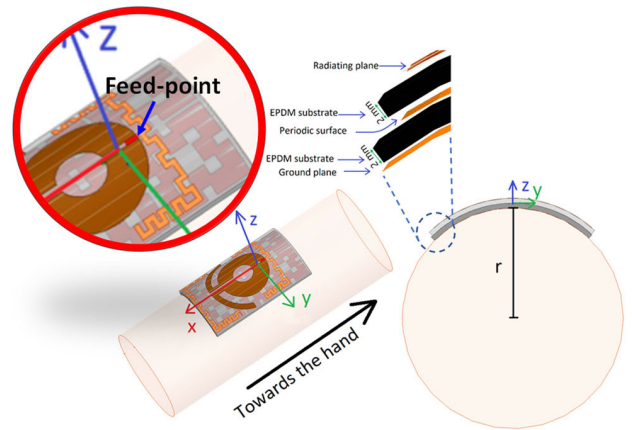

FIGURE 1. Wearable quasi-Yagi antenna mounted on the cylinder modelling the forearm (left side), the front view (right side) and exploded view of the model (top side).

Therefore, a simplistic approach is needed for modeling the electromagnetic properties of the wearable antenna effectively. To model the electromagnetic energy dissipation in the biological tissues and the relative permittivity, we used a homogenous forearm model comprising skin, which is comparatively nearest to the antenna and among most energy dissipative materials (σ = 0.855 S/m and ε_r = 41.85 at 915 MHz) [34]. The radius of the human forearm model estimates an average adult male. The radius and length of the cylinder was set to 46 mm and 250 mm, respectively. Figure 1 shows the forearm model, the antenna structure mounted on it, and the coordinate system which we will use throughout this work in the radiation pattern analysis.

The quasi-Yagi antenna is a planar, low-profile, structure that provides a directive end-fire beam in free space environment [32]. As shown in our previous work on the headgear RFID tag [32], in the wearable configuration, the end-fire radiation property can be restored by mounting the quasi-Yagi antenna on a periodic surface. Thus, we considered this configuration viable also for the forearm reader antenna.

The initial step of developing the quasi-Yagi antenna is considering the antenna geometry shown in Fig. 1 and Fig. 2. The quasi-Yagi antenna includes the driven element, typically a folded dipole, and parasitic elements operating as a reflector and directors. One of the most challenging tasks in this antenna development is to fit the antenna in the forearm's limited space and maintain the electrical length of 0.5λ or 80 mm of the antenna elements. To solve this, we applied the meandering and folding technique for all the antenna elements and reduced the element spacing as shown in Fig. 2. As a result, the total size of the radiator is 67 mm × 95 mm and the total lengths of the director and reflector is 243 mm (0.74λ) and 263 mm (0.8λ), respectively. The driven element was folded as two loops. The first loop with radius r_1 is optimized for impedance matching and the second loop with radius r_2 increases the total length of the driven element to 253 mm (0.77λ).

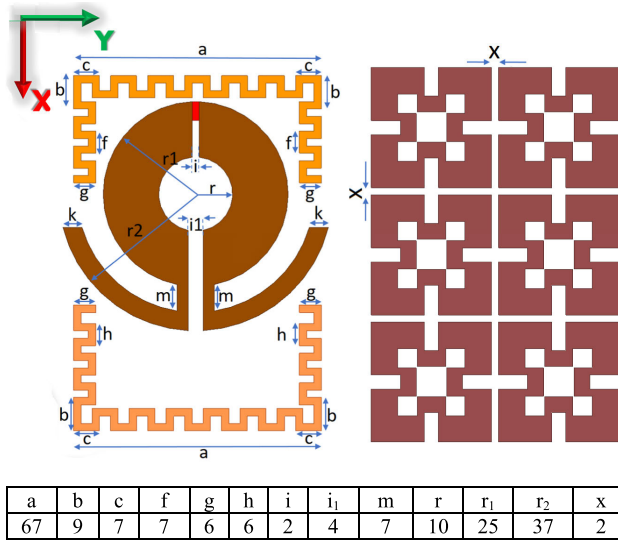| a	b	c	f	g	h	i	i_1	m	r	r_1	r_2	x
67	9	7	7	6	6	2	4	7	10	25	37	2

FIGURE 2. Top view of the quasi-Yagi antenna and periodic surface and the periodic surface with the geometrical parameters reported in millimeters.

The next step of developing the antenna on forearm is to optimize the periodic surface made up of a grid of unit cells. Following the principle from [35], we selected the non-grounded via-free configuration for the unit cells that instead of generating stop band for the surface-waves, enhances them and thereby is suitable for creating surface wave antennas. Considering the reflection phase criteria of $90° \pm 45°$ that was found to support the 50-Ω matching of wire type antenna on the periodic surface [36], we took this as the initial target. In addition to the surface-wave property, in our application the ground plane of the periodic surface helps to suppress the undesired antenna-body EM coupling.

As the unit cell structure, we selected the square loop configuration introduced in [46], because this unit cell type balances the simplicity of fabrication and the ease of adapting the geometry to obtain the targeted reflection phase. It was originally designed for 9.5 GHz, but the structure permits us to scale its dimensions to our target frequency of 915 MHz without increasing the size beyond with is feasible considering the size available on the forearm. The optimization of the unit cell geometry was done in ANSYS High-Frequency Structure Simulator (HFSS) v19.1, which is a full-wave electromagnetic field solver based on the finite element method, using the Floquet boundary condition (see Fig. 3). The target was obtaining the $90° \pm 45°$ reflection phase response in 915 MHz UHF RFID band. In the simulation, the impact of bending on unit cell reflection phase was also considered. We bent the unit cell with various radii of curvature realistic to our application and found the reflection phase to remain stable. The simulation model and the reflection phase are shown in Fig. 3 and the final layout of the unit cell is shown in Fig. 4. Next, considering the size of the forearm, we organized the unit cells into a 2-by-3 grid as shown Fig. 2 to form the periodic surface.
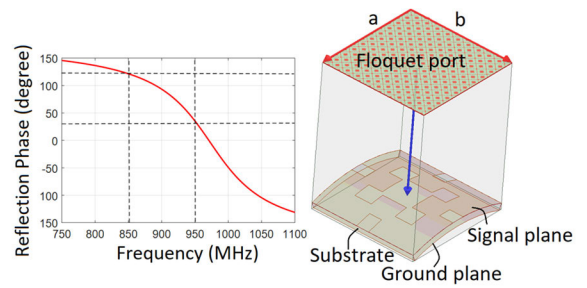

FIGURE 3. Floquet port simulation of the reflection phase of the periodic surface.

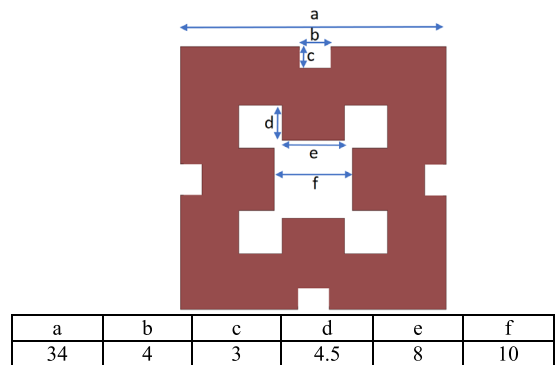| a	b	c	d	e	f
34	4	3	4.5	8	10

FIGURE 4. The unit cell of periodic surface with the geometrical parameters reported in millimeters.

Finally, we attached the radiating plane on top of the periodic surface and installed the whole antenna structure on the forearm model as shown in Fig. 1. From the cross-sectional view, the whole structure of the antenna consists of 5 layers (see Fig. 1). The first layer of the antenna is the radiating plane. The periodic surface layer was sandwiched between two textile layers of flexible, ethylene-propylene-diene-monomer (EPDM) rubber foam with a thickness of 2 mm ($\varepsilon_r = 1.53$, $\sigma = 0.01$ S/m [32]). The last layer is the ground plane that can isolate the antenna on the skin to prevent unexpected interaction between the human body and electromagnetic fields. The overall dimensions of the antenna are $0.22\lambda \times 0.33\lambda$.

We co-optimized the quasi-Yagi antenna and the periodic surface to achieve maximized realized gain and directivity exhibiting end-fire radiation pattern at 915 MHz frequency. To assess how close the directivity along the forearm (D_{arm}) comes to the peak value (D_{peak}) considering all spatial directions, we define $\Delta_{dir} = D_{arm}/D_{peak}$. In terms of our design, the target is to achieve $\Delta_{dir} = 1$ with as high as possible value of D_{peak}. Figure 5(a) shows Δ_{dir} and the quasi-Yagi antenna's peak directivity with and without the periodic surface. From the results, it is evident that without the periodic surface both D_{peak} and Δ_{dir} are tending toward local minima near the targeted 915 MHz UHF RFID band and the insertion of the periodic surface reverses this, so that the quantities attain local maxima instead, as desired. With the periodic surface we have $D_{peak} = 5.9$ dBi and $D_{arm} = 5.3$ dBi.
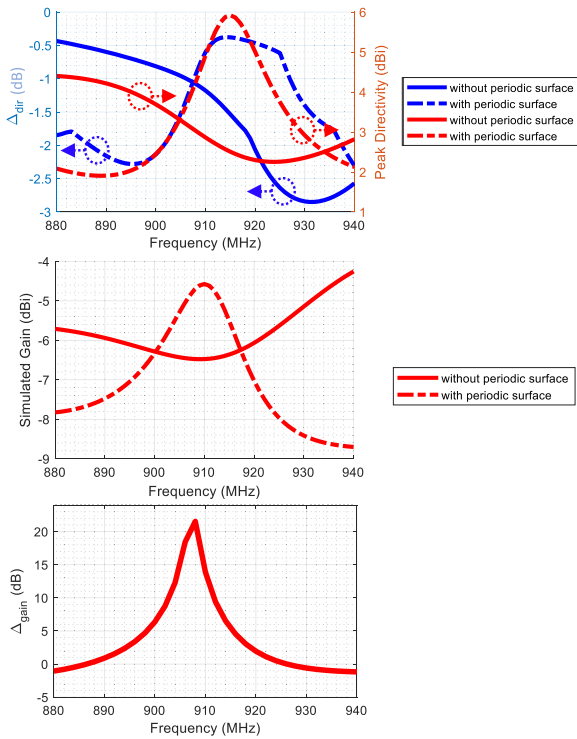
FIGURE 5. (a) Peak directivity, delta, and (b) gain of the quasi-Yagi reader antenna with and without periodic surface (c) front to back lobe ratio for simulated gain.
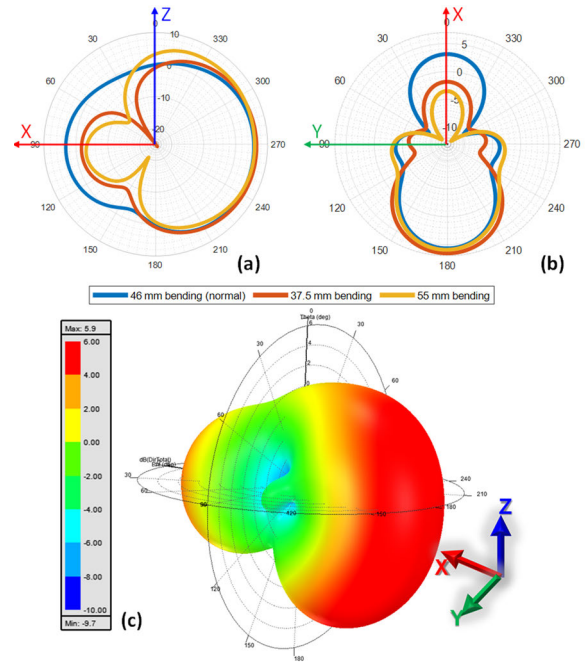

FIGURE 6. Directivity pattern in (a) XZ and (b) XY planes. (c) simulated 3D directivity pattern of quasi-Yagi antenna exhibiting end-fire radiation properties in the forearm direction (46 mm bending).

Correspondingly, Fig. 5(b) shows a comparison of the simulated gain, with and without the periodic surface, where the gain with the periodic surface is improved to a value of −5.5 dBi in the forearm direction. We defined Δ_{gain} as the ratio G_{front}/G_{back}, where the G_{front} and G_{back} is the gain in $(\theta = 90°, \varphi = 180°)$ and $(\theta = 90°, \varphi = 0°)$ directions, respectively. In Fig. 5(c), Δ_{gain} achieves a value of 5 dB at 915 MHz frequency indicating that maximum power is radiated in the − x direction i.e. away from the person wearing the antenna (Fig. 1).

As discussed earlier, the curvature of the forearm defines the bending degree of the antenna and may vary with the body anatomy, we have considered various radii of the human forearm i.e. *r* varies between 37.5 mm and 55 mm. Fig. 6(a) and Fig. 6(b) shows the 2D directivity pattern of the quasi-Yagi antenna in XZ and XY planes, respectively. Figures also elaborates the impact of bending on the antenna's peak directivity. Although the bending does not significantly impact the peak directivity or Δ_{dir} of the antenna and the reflection phase of the periodic surface, yet the end-fire radiation defined by Δ_{gain} property is improved with various bending degrees i.e. the back lobe reduces significantly. Fig. 6(c) shows the 3D directivity pattern of the quasi-Yagi antenna exhibiting the end-fire directivity pattern of the antenna along the direction of the arm $(\theta = 270°, \varphi = 180°)$ with a peak directivity of −5.9 dBi.

The reader quasi-Yagi antenna without the periodic surface exhibits input impedance of *48 + 82j* Ω, as shown

in the Fig. 7(a). However, the periodic surface directs the peak surface current of 49 A/m into driver of the quasi-Yagi antenna, achieving the end-fire radiation characteristics for the antenna. Figure 8 shows the surface with and without the periodic surface when 1 W of power is fed to the antenna. With the periodic surface, the antenna exhibits input impedance of *4 + 25j* Ω, as shown in Fig. 7(a). As the primary objective of our work is to achieve the end-fire radiation properties, we have used a matching circuit designed in Advanced Design System (ADS), shown in the Fig. 7(b), to resonate the antenna at the 915 MHz frequency. We also studied the impact of various curvature of the human forearm on the resonance frequency of the antenna. Figure 9 shows the simulated reflection coefficient of the antenna mounted on various forearm sizes. The antenna resonates at 915 MHz with a reflection coefficient of −25 dB at standard bending of 46 mm. The simulation results also show that the antenna's frequency bandwidth splits into a dual band with the change in the bending curvature. However, the targeted frequency of 915 MHz remains inside the −10 dB S_{11} bandwidth under the various curvatures of the forearm.

For the antennas operation in the human body's proximity, the transmission power is limited by the specific absorption rate and is regulated by the US FCC [37], limiting SAR to 1.6 W/kg averaged over 1 g of tissues. Consequently, to determine the maximum SAR complaint transmission power ($P_{t,max}$) for the quasi-Yagi reader antenna is expressed as [38]

$$P_{t,max} = \frac{1.6W/kg \left(1 - |S_{11}|^2\right) P_{test}}{SAR_{max}}, \quad (1)$$
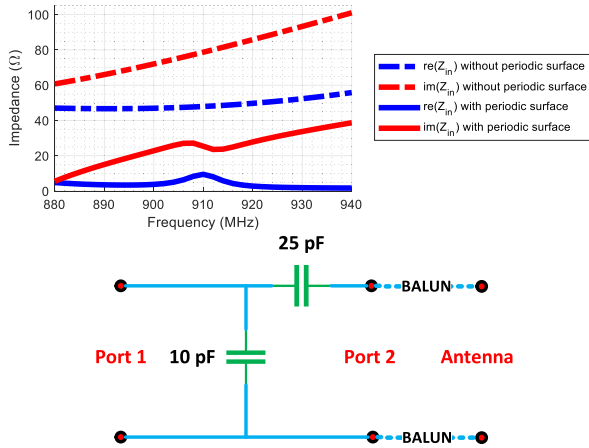
FIGURE 7. (a) Input impedance of the antenna with and without the periodic surface (b) schematic of the matching circuit designed to resonate the antenna at 915 MHz frequency.
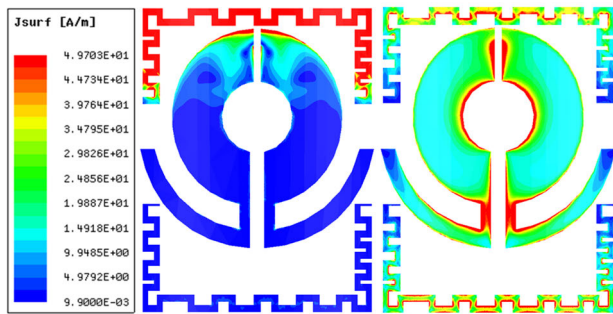

FIGURE 8. Surface current distribution at the quasi-Yagi antenna with and without the periodic surface (left to right).

where P_{test} is the power available from the numerical test source that we set to 1 W. In the simulation, the maximum SAR that occurs in the tissue nearest to the radiating antenna is 0.9 W/kg, and the maximum SAR compliant transmission power is calculated as 41.2 dBm using (1). This is comparatively higher than reported in the previous works, indicating our antenna exhibits lower SAR. Considering the emission limits of EIRP = 3.28 W or EIRP = 4 W set for UHF RFID systems, the antenna could transmit 40.6 dBm or 41.5 dBm, respectively. Overall, we conclude the that the output power is limited nearly equally by both, the SAR and emission limits. However, this output power limit is notably high and especially for mobile RFID reader units, the output power is expected to be an order of lower magnitude. Thus, in the wireless testing we present in Section IV, we have used the output power of 32 dBm.

III. TEST TAG FOR THE READER ANTENNA CHARACTERIZATION

One of the most significant parameters of a body-worn antenna is its realized gain, which is determined by the input reflection coefficient, directivity, and the radiation efficiency of the antenna. However, the measurement of the
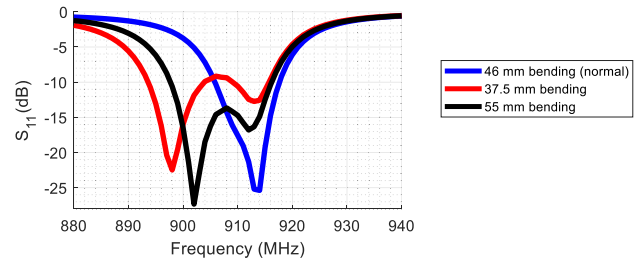

FIGURE 9. Reflection coefficient of the quasi-Yagi antenna mounted on various forearm sizes.

realized gain a wearable antenna in body-worn configuration by using conventional techniques becomes significantly difficult. Therefore, in this work we have adopted an alternative approach applicable specifically to RFID reader antennas by utilizing an RFID tag analogous to the reference gain antenna in the classical far field antenna measurement.

For this purpose, we have first designed and implemented a dipole type test tag antenna shown in Fig. 10. The test tag was designed based on the regular embedded inductive loop matching method [39]. The main target of the design was to achieve the antenna input impedance that equals the complex conjugate impedance of the NXP UCODE G2iL series RFID IC [40] having the turn on power of $P_{ic0} = -18$ dBm. For this purpose, the antenna geometry (primarily the parameters L_{s1}, W_{s1} and W_{s2}) was adapted in ANSYS High-Frequency Structure Simulator (HFSS) v19.1. The impedance of the chip was estimated by using an equivalent circuit comprising capacitance and resistance connected in parallel [28].
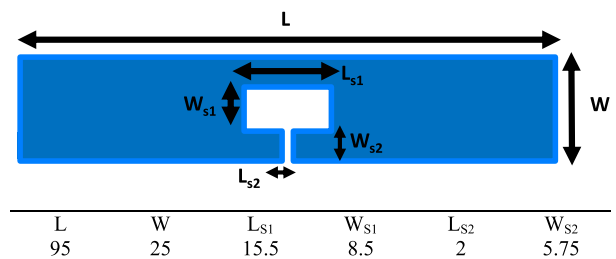

L	W	L_{S1}	W_{S1}	L_{S2}	W_{S2}
95	25	15.5	8.5	2	5.75

FIGURE 10. Structure of the test tag antenna and its dimensional parameters given in millimeters.

The manufactured test tag was characterized using Voyantic Tagformance Pro measurement system [27]. For the characterization of fully assembled UHF RFID tags, the system enables the recording of the lowest continuous-wave output power (threshold power: P_{th}) of the reader for which the tag under test backscatters a valid 16-bit random number as a response to the reader's query command in ISO 18000-6C communication standard. It also provides the estimation of the path loss factor L_{iso} from the device output to the location of the tag under test. This is achieved through the threshold power measurement performed on the manufacturer's system reference tag with accurately known properties that enable the computation of L_{iso}. This enables us to compute the realized

TABLE 2. Comparison with the contemporary research work.

Ref.	Freq. (GHz)	Gain (dBi)	Size (mm)	Thickness (mm)	Relative size	Read range (m)*	RFID reader	Pattern type
[28]	0.866	−4	80×62	4	0.23×0.18 λ_o	1.5	Yes	1
[26]	0.866	2	80×70	1.52	0.23×0.20 λ_o	1.45	Yes	2
[31]	0.880	−5	63×65	--	0.18×0.19 λ_o	2	Yes	1
[42]	0.866	−1.31	140×100	4	0.40×0.29 λ_o	2.3	Yes	1
[45]	0.915	−10.9	360×360	5	1.19×1.1 λ_o	2.1	No	1
[47]	2.47	0.1	50×50	9.5	0.41×0.41 λ_o	1.29	No	2
[48]	0.860	1	90×49	4	0.25×0.14 λ_o	4.23	No	1
[49]	0.868	−2.6	87×77	4	0.25×0.22 λ_o	2.76	No	1
Our work	0.915	−5.5	67×108	4	0.22×0.33 λ_o	2	Yes	2

*Estimated read ranges (S_{max}) based on the test tag used in our work $(P_{rx} = -18$ dBm) and calculated by equation (5) assuming $P_{tx} = 25$ dBm.
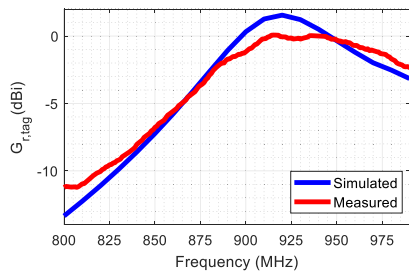

FIGURE 11. Measured and simulated realized gain of the test tag antenna.

FIGURE 12. Matching network, balun, and the antenna connection configuration for the reflection coefficient measurement (left), and the fabricated wearable quasi-Yagi reader antenna (right).

gain $G_{r,tag}$ of the test tag antenna as detailed in [40]

$$G_{r,tag} = \frac{P_{ic0}}{L_{iso}P_{th}}, \qquad (2)$$

where P_{th} is the threshold power of the test tag. Fig. 15(a) shows the measurement setup for the characterization of the test tag. First the Tagformance is calibrated using the reference tag and later, the test tag is measured. As seen from the results in Fig. 11, the realized gain versus frequency peaks at 915 MHz, as desired, with the simulated and measured values of 1 dBi and 0 dBi, respectively. Later, we will utilize the measured realized gain of the test tag in the characterization of the quasi-Yagi reader antenna and to demonstrate the attainable read range of a common RFID tag.

IV. READER ANTENNA MEASUREMENT AND RESULTS

As the primary aim of our work is to demonstrate the end-fire radiation property of the reader antenna achieved by utilizing the periodic surface, the reader antenna is not self-matched to 50 Ω. Thus, a matching circuit is used to match the input impedance of the reader antenna to the standard 50 Ω impedance. To achieve this, we first measured the feed-point impedance of the antenna $(8 + 9j$ Ω at 915 MHz) through a balun made-up of a coaxial cable. The impedance of the antenna through a balun made-up of coaxial cable (see Fig. 13), that suppresses the common mode currents as the driven element of the quasi-Yagi antenna is a dipole (differential antenna) [42]. After this we developed a simple two-component L-matching circuit [43] that is shown in Fig. 12 to transform the antenna's feedpoint impedance
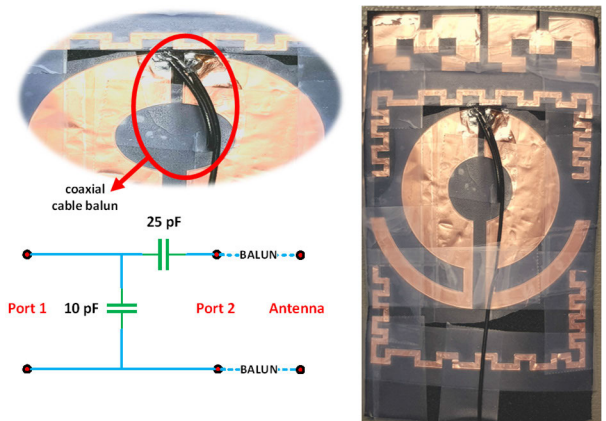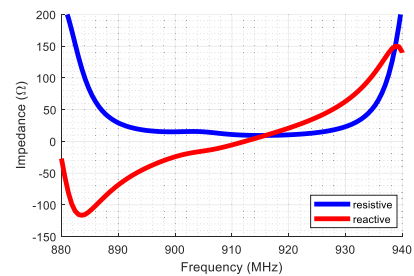

FIGURE 13. Input impedance of the antenna before matching network.

of $8 + 9j$ Ω at 915 MHz to the input impedance of 50 Ω seen through the matching circuit. As seen from Fig. 13, both the simulation and measurement show that the matching circuit provides the desired impedance transformation at 915 MHz.

Next, we measured the realized gain (G_R) of the wearable quasi-Yagi antenna using the test tag presented in Section III. In the experimental arrangement shown in Fig. 15b, the reader antenna was attached on the forearm which was pointed towards the test tag that was placed at distance of 1 meter from the reader antenna. In the experiment the reader antenna was placed directly on the skin to achieve an identical scenario to the simulation. We then connected the reader antenna to the
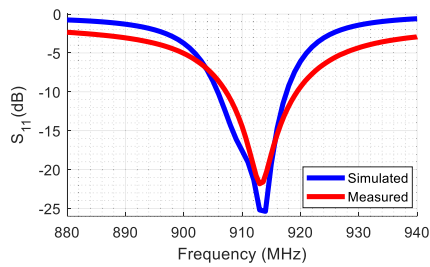
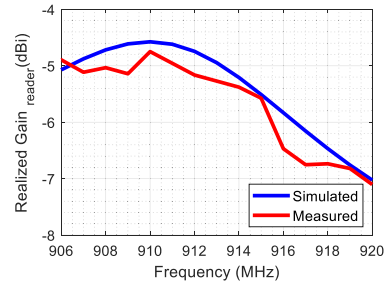**FIGURE 14.** Simulated and measured reflection coefficient of the quasi-Yagi antenna in body worn condition.

FIGURE 16. Realized gain of the quasi-Yagi reader antenna in the body-worn configuration.
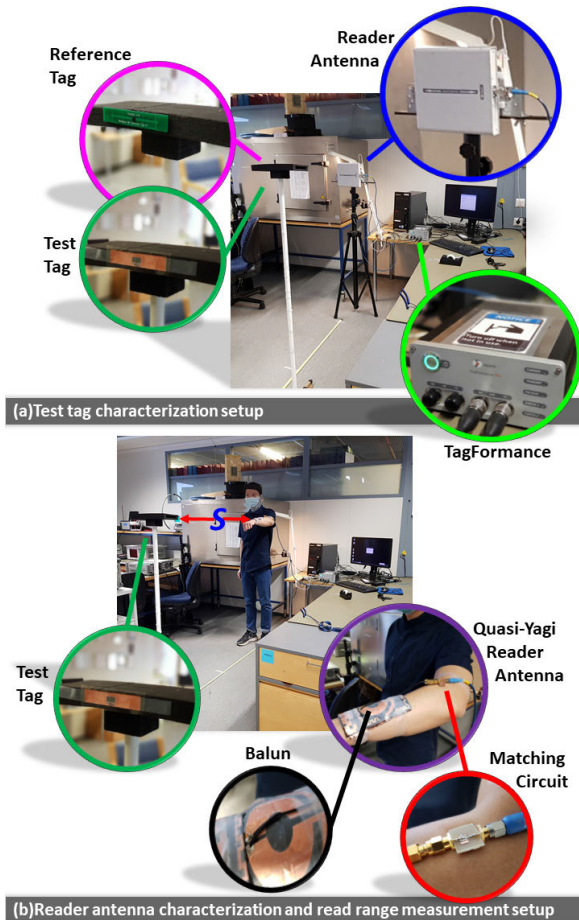

FIGURE 15. The measurement setup for (a) test tag antenna characterization (b) reader antenna characterization and read range measurement.

Voyantic Tagformance Pro measurement system introduced in Section III and recorded the threshold power of the test tag using the wearable reader. This enables us to solve the realized gain of the wearable quasi-Yagi reader antenna (G_R) from Friis' transmission formula

$$P_{rx} = G_R G_{r,tag} L_{cab} \left(\frac{\lambda}{4\pi s} \right)^2 P_{tx}, \qquad (3)$$

where $L_{cab} = -1.1$ dB is the power loss factor, we measured for the cable connecting the quasi-Yagi antenna to the

RF output of the Tagformance device. For comparison, the simulated realized gain of the reader antenna is given by

$$G_R = G \left(1 - |s_{11}|^2 \right), \qquad (4)$$

where G and s_{11} are the simulated gain and reflection coefficient of the quasi-Yagi antenna. In Fig. 16, the simulated realized gain shows good agreement with the calculated realized gain over the -10 dB S_{11}-bandwidth of the antenna at the end-fire direction (see Fig. 14). The measured realized gain of the quasi-Yagi antenna is -5.5 dBi at the operating frequency of 915 MHz. To estimate the corresponding attainable tag read range versus transmission power, we varied the transmission power P_{tx}, so that, the power delivered to the quasi-Yagi antenna ($P_{tx}L_{cab}$) was between 5 dBm and 32 dBm. We then manually moved the test tag further away from the reader antenna and measured the critical antenna separation (s_{max}) that corresponds with the scenario that the tag antenna captures barely enough power to turn on the RFID IC; i.e. $P_{rx} = P_{ic0} - 18$ dBm. This distance is the attainable read range of the tag for a given transmission power. For the comparison with the simulation, we have

$$s_{max} = \frac{\lambda}{4\pi} \sqrt{\frac{G_{r,tag} G_R L_{cab} P_{tx}}{P_{rx}}}, \qquad (5)$$

from equation (3) and we can compute s_{max} using the simulated realized gains of the test tag and the quasi-Yagi reader antenna. Fig. 17 shows the results. The measured and calculated read range shows good agreement with an approximately constant relative difference that is 150 cm at 32 dBm transmission power. Since both graphs show the same trend versus the transmission power, we expect the difference to the primarily due to the lower measured realized gains of the tag and reader antennas as compared with the simulation and not because of multipath propagation effects.

Table 2 summarizes some of the contemporary wearable reader antennas with estimated attainable read ranges for the test tag, introduced in the section III. We calculated the attainable read ranges of the wearable antenna through equation (5), when 25 dBm transmission power is fed to the antenna. Moreover, we classified the antennas based on the radiation pattern to Type 1 and Type 2, which denote radiation
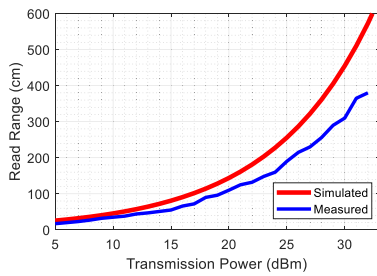
to an off-body direction and along the body surface, respectively. Even though the antennas from several other works, especially [26], [47], and [48], provide notably high gain, among the radiation pattern Type 2 antennas, our antenna provides the highest read range. However, it should be noted that the antenna [47] is not originally proposed as a reader antenna, operates at 2.47 GHz and thus it's hypothetical read range is affected also by the shorter operating wavelength.

V. CONCLUSION

Wearable antennas are fundamental to smart clothing in wireless body-area systems. We have presented, a metasurface-enabled quasi-Yagi UHF RFID reader antenna worn on the forearm and optimized to detect RFID tags in the pointing direction of the arm. The antenna that conforms on the forearm, comprises two layers of low-permittivity textile material, where the bottom layer is a periodic surface on a ground plane. The top layer that carries the quasi-Yagi radiator, is suspended on the periodic surface. Due to the body proximity, the quasi-Yagi radiator alone does not provide end-fire radiation along the body surface, but by co-optimizing the periodic surface for the enhanced launching of the surface waves with the quasi-Yagi radiator, we achieved the end-fire directivity of 5.5 dBi. The ground plane of the periodic surface also decouples the radiator from the body and reduces the SAR. Our simulations showed that the maximum SAR-compliant power of the antenna is 41 dBm, which is an order of magnitude higher than a typical output power level of a mobile RFID reader. In our practical testing, we were able to detect a regular dipole type RFID tag at 3.8 meters with the reader's output power of 32 dBm (EIRP = 0.56 W) at 915 MHz.

ACKNOWLEDGMENT

REFERENCES

[1] S. Genovesi, F. Costa, M. Borgese, F. A. Dicandia, A. Monorchio, and G. Manara, "Chipless RFID sensor for rotation monitoring," in *Proc. IEEE Int. Conf. RFID Technol. Appl. (RFID-TA)*, Warsaw, Poland, Sep. 2017, pp. 233–236.

[2] H. He, X. Chen, L. Ukkonen, and J. Virkki, "Clothing-integrated passive RFID strain sensor platform for body movement-based controlling," in *Proc. IEEE Int. Conf. RFID Technol. Appl. (RFID-TA)*, Pisa, Italy, Sep. 2019, pp. 236–239.

[3] S. Amendola, L. Bianchi, and G. Marrocco, "Movement detection of human body segments: Passive radio-frequency identification and machine-learning technologies," *IEEE Antennas Propag. Mag.*, vol. 57, no. 3, pp. 23–37, Jun. 2015.

[4] H. Ding, J. Han, L. Shangguan, W. Xi, Z. Jiang, Z. Yang, Z. Zhou, P. Yang, and J. Zhao, "A platform for free-weight exercise monitoring with passive tags," *IEEE Trans. Mobile Comput.*, vol. 16, no. 12, pp. 3279–3293, Dec. 2017.

[5] A. E. Abdulhadi and T. A. Denidni, "Self-powered multi-port UHF RFID Tag-Based-Sensor," *IEEE J. Radio Freq. Identificat.*, vol. 1, no. 2, pp. 115–123, Jun. 2017.

[6] J. Zhang, X. Wang, Z. Yu, Y. Lyu, S. Mao, S. C. Periaswamy, J. Patton, and X. Wang, "Robust RFID based 6-DoF localization for unmanned aerial vehicles," *IEEE Access*, vol. 7, pp. 77348–77361, Jun. 2019.

[7] L. Shen, Q. Zhang, J. Pang, H. Xu, and P. Li, "PRDL: Relative localization method of RFID tags via phase and RSSI based on deep learning," *IEEE Access*, vol. 7, pp. 20249–20261, Jan. 2019.

[8] A. Fahim, T. Elbatt, A. Mohamed, and A. Al-Ali, "Towards extended bit tracking for scalable and robust RFID tag identification systems," *IEEE Access*, vol. 6, pp. 27190–27204, May 2018.

[9] F. Xiao, Z. Wang, N. Ye, R. Wang, and X.-Y. Li, "One more tag enables fine-grained RFID localization and tracking," *IEEE/ACM Trans. Netw.*, vol. 26, no. 1, pp. 161–174, Feb. 2018.

[10] X. Liu, X. Xie, K. Li, B. Xiao, J. Wu, H. Qi, and D. Lu, "Fast tracking the population of key tags in large-scale anonymous RFID systems," *IEEE/ACM Trans. Netw.*, vol. 25, no. 1, pp. 278–291, Feb. 2017.

[11] A. Sani, M. Rajab, R. Foster, and Y. Hao, "Antennas and propagation of implanted RFIDs for pervasive healthcare applications," *Proc. IEEE*, vol. 98, no. 9, pp. 1648–1655, Sep. 2010.

[12] R. Lodato, V. Lopresto, R. Pinto, and G. Marrocco, "Numerical and experimental characterization of through-the-body UHF-RFID links for passive tags implanted into human limbs," *IEEE Trans. Antennas Propag.*, vol. 62, no. 10, pp. 5298–5306, Oct. 2014.

[13] R. C. Hadarig, M. E. de Cos, and F. Las-Heras, "UHF dipole-AMC combination for RFID applications," *IEEE Antennas Wireless Propag. Lett.*, vol. 12, pp. 1041–1044, Aug. 2013.

[14] M. A. S. Tajin and K. R. Dandekar, "Pattern reconfigurable UHF RFID reader antenna array," *IEEE Access*, vol. 8, pp. 187365–187372, Oct. 2020.

[15] Y. Kuang, L. Yao, W. Zhang, D. Zhou, H. Luan, and Y. Qiu, "A novel textile dual-polarized antenna potentially used in body-centric system," in *Proc. IEEE Int. Conf. RFID Technol. Appl. (RFID-TA)*, Foshan, China, Sep. 2016, pp. 77–80.

[16] E. Moradi, L. Sydanheimo, G. S. Bova, and L. Ukkonen, "Measurement of wireless power transfer to deep-tissue RFID-based implants using wireless repeater node," *IEEE Antennas Wireless Propag. Lett.*, vol. 16, pp. 2171–2174, May 2017.

[17] J. J. Baek, S. W. Kim, K. H. Park, M. J. Jeong, and Y. T. Kim, "Design and performance evaluation of 13.56-MHz passive RFID for E-Skin sensor application," *IEEE Microw. Wireless Compon. Lett.*, vol. 28, no. 12, pp. 1074–1076, Dec. 2018.

[18] G. Scotti, S.-Y. Fan, C.-H. Liao, and Y. Chiu, "Body-implantable RFID tags based on ormocer printed circuit board technology," *IEEE Sensors Lett.*, vol. 4, no. 8, pp. 1–4, Aug. 2020.

[19] C. Miozzi, S. Nappi, S. Amendola, C. Occhiuzzi, and G. Marrocco, "A general-purpose configurable RFID epidermal board with a two-way discrete impedance tuning," *IEEE Antennas Wireless Propag. Lett.*, vol. 18, no. 4, pp. 684–687, Apr. 2019.

[20] I. Bouhassoune, R. Saadane, and A. Chehri, "Wireless body area network based on RFID system for healthcare monitoring: Progress and architectures," in *Proc. 15th Int. Conf. Signal-Image Technol. Internet-Based Syst. (SITIS)*, Sorrento, Italy, Nov. 2019, pp. 416–421.

[21] H. Xiaomu, S. Yan, and G. A. E. Vandenbosch, "Wearable button antenna for dual-band WLAN applications with combined on and off-body radiation patterns," *IEEE Trans. Antennas Propag.*, vol. 65, no. 3, pp. 1384–1387, Mar. 2017.

[22] C. Mao, P. L. Werner, and D. H. Werner, "Low-profile textile antenna with omni-directional radiation for wearable applications," in *Proc. Int. Appl. Comput. Electromagn. Soc. Symp. (ACES)*, Miami, FL, USA, Apr. 2019, pp. 1–2.

[23] S. Kumar, P. Ranjan, S. Arava, K. P. Kalyan, and T. S. Chand, "Design and analysis of dielectric resonator antenna for wearable applications," in *Proc. Int. Conf. Vis. Towards Emerg. Trends Commun. Netw. (ViTECoN)*, Vellore, India, Mar. 2019, pp. 1–3.

[24] F. Lagha, S. Beldi, and L. Latrach, "Design of UHF RFID body-worn textile tag for wireless applications," in *Proc. IEEE Int. Conf. Design Test Integr. Micro Nano-Syst. (DTS)*, Gammarth-Tunis, Tunisia, Apr. 2019, pp. 1–4.

[25] H. He, X. Chen, O. Mokhtari, H. Nishikawa, L. Ukkonen, and J. Virkki, "Fabrication and performance evaluation of carbon-based stretchable RFID tags on textile substrates," in *Proc. Int. Flexible Electron. Technol. Conf. (IFETC)*, Ottawa, ON, Canada, Aug. 2018, pp. 1–5.

[26] K. Jebbawi, M. Egels, and P. Pannier, "Design of an ultra-wideband UHF RFID reader antenna for wearable ankle tracking applications," in *Proc. Eur. Microw. Conf. Central Eur. (EuMCE)*, Prague, Czech Republic, May 2019, pp. 525–528.

[27] M. Daiki and E. Perret, "Segmented solenoid coil antenna for UHF RFID near-field reader applications," *IEEE J. Radio Freq. Identificat.*, vol. 2, no. 4, pp. 210–218, Dec. 2018.

[28] S. Ahmed, S. T. Qureshi, L. Sydanheimo, L. Ukkonen, and T. Bjorninen, "Comparison of wearable E-textile split ring resonator and slotted patch RFID reader antennas embedded in work gloves," *IEEE J. Radio Freq. Identificat.*, vol. 3, no. 4, pp. 259–264, Dec. 2019.

[29] R. K. Singh, A. Michel, P. Nepa, and A. Salvatore, "Glove integrated dual-band Yagi reader antenna for UHF RFID and Bluetooth application," in *Proc. Int. Workshop Antenna Technol. (iWAT)*, Bucharest, Romania, Feb. 2020, pp. 1–3.

[30] A. S. Andrenko, Y. Shimizu, and K. Wake, "SAR measurements of UHF RFID reader antenna operating in close proximity to a flat phantom," in *Proc. IEEE Int. Conf. RFID Technol. Appl. (RFID-TA)*, Pisa, Italy, Sep. 2019, pp. 297–300.

[31] R. K. Singh, A. Michel, P. Nepa, and A. Salvatore, "Compact Quasi-Yagi reader antenna for UHF RFID smart-glove," in *Proc. 5th Int. Conf. Smart Sustain. Technol. (SpliTech)*, Split, Croatia, Sep. 2020, pp. 1–4.

[32] N. Kaneda, W. R. Deal, Y. Qian, R. Waterhouse, and T. Itoh, "A broadband planar Quasi-Yagi antenna," *IEEE Trans. Antennas Propag.*, vol. 50, no. 8, pp. 1158–1160, Aug. 2002.

[33] D. Le, L. Ukkonen, and T. Bjorninen, "A dual-ID RFID tag for head-gear based on Quasi-Yagi and dipole antennas," *IEEE Antennas Wireless Propag. Lett.*, vol. 19, no. 8, pp. 1321–1325, Aug. 2020.

[34] *IT'IS Foundation, Tissue Properties*. Accessed: Apr. 5, 2021. [Online]. Available: https://www.itis.ethz.ch/virtual-population/tissue-properties/downloads

[35] F. Yang, A. Aminian, and Y. Rahmat-Samii, "A novel surface-wave antenna design using a thin periodically loaded ground plane," *Microw. Opt. Technol. Lett.*, vol. 47, no. 3, pp. 240–245, Nov. 2005.

[36] F. Yang and Y. Rahmat-Samii, "Reflection phase characterizations of the EBG ground plane for low profile wire antenna applications," *IEEE Trans. Antennas Propag.*, vol. 51, no. 10, pp. 2691–2703, Oct. 2003.

[37] *Radiofrequency Radiation Exposure Evaluation: Portable Devices*, U.S. Code of Federal Regulations 47, document CFR 2.1093, Oct. 2010.

[38] E. Moradi, S. Amendola, T. Bjorninen, L. Sydanheimo, J. M. Carmena, J. M. Rabaey, and L. Ukkonen, "Backscattering neural tags for wireless brain-machine interface systems," *IEEE Trans. Antennas Propag.*, vol. 63, no. 2, pp. 719–726, Feb. 2015.

[39] G. Marrocco, "The art of UHF RFID antenna design: Impedance-matching and size-reduction techniques," *IEEE Antennas Propag. Mag.*, vol. 50, no. 1, pp. 66–79, Feb. 2008.

[40] T. Björninen, L. Sydänheimo, and L. Ukkonen, "Development and validation of an equivalent circuit model for UHF RFID IC based on wireless tag measurements," in *Proc. Antenna Meas. Techn. Assoc. Symp.*, Bellevue, WA, USA, Oct. 2012, pp. 480–485.

[41] *NXP Semiconductors, Eindhoven, Netherlands, UCODE G2iL(+) Series ICs*. Accessed: Apr. 6, 2021. [Online]. Available: http://www.nxp.com/products/identification_and_security/smart_label_and_tag_ics/ucode/

[42] R. Bourtoutian, C. Delaveaud, and S. Toutain, "Differential antenna design and characterization," in *Proc. 3rd Eur. Conf. Antennas Propag.*, Berlin, Germany, Mar. 2009, pp. 2398–2402.

[43] D. M. Pozar, *Microwave Engineering*, 4th ed. Hoboken, NJ, USA: Wiley, 2012.

[44] S. Ahmed, A. Mehmood, L. Sydanheimo, L. Ukkonen, and T. Bjorninen, "Glove-integrated textile antenna with reduced SAR for wearable UHF RFID reader," in *Proc. IEEE Int. Conf. RFID Technol. Appl. (RFID-TA)*, Pisa, Italy, Sep. 2019.

[45] H. Lee, J. Tak, and J. Choi, "Wearable antenna integrated into military berets for indoor/outdoor positioning system," *IEEE Antennas Wireless Propag. Lett.*, vol. 16, pp. 1919–1922, 2017.

[46] A. Foroozesh and L. Shafai, "Investigation into the application of artificial magnetic conductors to bandwidth broadening, gain enhancement and beam shaping of low profile and conventional monopole antennas," *IEEE Trans. Antennas Propag.*, vol. 59, no. 1, pp. 4–20, Jan. 2011.

[47] K. Agarwal, Y.-X. Guo, and B. Salam, "Wearable AMC backed near-endfire antenna for on-body communications on latex substrate," *IEEE Trans. Compon., Packag., Manuf. Technol.*, vol. 6, no. 3, pp. 346–358, Mar. 2016.

[48] C. Occhiuzzi, S. Cippitelli, and G. Marrocco, "Modeling, design and experimentation of wearable RFID sensor tag," *IEEE Trans. Antennas Propag.*, vol. 58, no. 8, pp. 2490–2498, Aug. 2010.

[49] G. A. Casula, G. Montisci, and H. Rogier, "A wearable textile RFID tag based on an eighth-mode substrate integrated waveguide cavity," *IEEE Access*, vol. 8, pp. 11116–11123, Jan. 2020.

SHAHBAZ AHMED (Student Member, IEEE) received the B.E. degree in electronics engineering from AIR University, Islamabad, Pakistan, in 2013, and the M.Sc. degree in electrical engineering with major in electronics from Tampere University, Tampere, Finland, in 2018, where he is currently pursuing the Ph.D. degree with the Wireless Identification and Sensing Systems Research Group.

He has been a Network Support Engineer with Alcatel Lucent, Pakistan. His research interests include antenna designing, electromagnetic modeling, implantable and wearable biomedical systems, RFID systems, and low-profile antennas. He was a recipient of the Nokia Foundation Scholarship and the Finnish Foundation for Technology Promotion (Tekniikan edistämissäätiö) to support his research studies in the chosen area of interest.

DUC LE (Student Member, IEEE) received the B.S. degree (Hons.) in electrical engineering from the HCMC University of Technology and Education, Ho Chi Minh, Vietnam, in 2014, and the M.S. degree (Hons.) in electrical engineering from the Tampere University of Technology, Tampere, Finland, in 2018, where he is currently pursuing the Ph.D. degree with the Wireless Identification and Sensing Group. He was a Research Assistant with the Tampere University of Technology, from 2016 to 2018. His research interests include technology for wireless health, wearable antenna development, electromagnetic modelling, RF circuits, RFID tag, and low-profile antennas. He was a recipient of prestigious award, including the HPY Research Foundation of Elisa and the Nokia Foundation Scholarship to support research studies of telecommunications technology, studies closely related to telecommunications.

LAURI SYDÄNHEIMO (Member, IEEE) received the M.Sc. and Ph.D. degrees in electrical engineering from the Tampere University of Technology (TUT), Tampere, Finland. He is currently a Professor with the Faculty of Biomedical Sciences and Engineering, TUT. He has authored more than 200 publications in radio-frequency identification tag, reader antenna design, and wireless system performance improvement. His current research interests include wireless data communication and wireless identification and sensing.

LEENA UKKONEN (Member, IEEE) received the M.Sc. and Ph.D. degrees in electrical engineering from the Tampere University of Technology, Tampere, Finland, in 2003 and 2006, respectively. She is currently a Professor with the Faculty of Medicine and Health Technology, Tampere University, Tampere. She is leading the Wireless Identification and Sensing Systems Research Group. She has authored more than 300 scientific publications in radiofrequency identification (RFID), antenna design, and biomedical and wearable sensors. Her current research interests include RFID antennas, RFID sensors, implantable biomedical systems, and wearable antennas.

TONI BJÖRNINEN (Senior Member, IEEE) received the M.Sc. and Ph.D. degrees in electrical engineering from the Tampere University of Technology, Tampere, Finland, in 2009 and 2012, respectively.

He is currently an Academy of Finland Research Fellow with the Faculty of Medicine and Health Technology, Tampere University, Tampere. He has been a Visiting Postdoctoral Scholar with the Berkeley Wireless Research Center, UC Berkeley, and with the Microwave and Antenna Institute in Electronic Engineering Department, Tsinghua University, Beijing. He has coauthored 178 peer-reviewed scientific publications and given over 50 presentations in scientific symposia worldwide. His research interest includes microwave technology for wireless health, including implantable and wearable antennas, wireless power transfer, sensors, and RFID-inspired wireless solutions.

Dr. Björninen was a member of the editorial boards of *International Journal of Antennas and Propagation*, from 2014 to 2018, *IET Electronics Letters*, from 2016 to 2018, and IEEE JOURNAL OF RADIO FREQUENCY IDENTIFICATION, from 2017 to 2020. He is serving as an Associate Editor for *Applied Computational Electromagnetics Society Journal*.

• • •